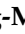



Article

Effect of Particle Size on the Mechanical Properties of TiO₂–Epoxy Nanocomposites

Young-Min Choi ^{1,†}, Seon-Ae Hwangbo ^{2,†}, Tae Geol Lee ² and Young-Bog Ham ^{1,*}

¹ Department of Thermal Systems, Korea Institute of Machinery and Materials, Daejeon 34103, Korea; anaud007@kimm.re.kr

² Nanosafety Team, Safety Measurement Institute, Korea Research Institute of Standards and Science, Daejeon 34113, Korea; hbsa@kriss.re.kr (S.-A.H.); tglee@kriss.re.kr (T.G.L.)

* Correspondence: hyb665@kimm.re.kr; Tel.: +82-042-868-7157

† These authors contributed equally to the work.

Abstract: This study investigated the effects of the packing density and particle size distribution of TiO₂ nanoparticles on the mechanical properties of TiO₂–epoxy nanocomposites (NCs). The uniform dispersion and good interfacial bonding of TiO₂ in the epoxy resin resulted in improved mechanical properties with the addition of nanoparticles. Reinforcement nano-TiO₂ particles dispersed in deionized water produced by three different ultrasonic dispersion methods were used; the ultrasonication effects were then compared. The nano-TiO₂ suspension was added at 0.5–5.0 wt.%, and the mechanical and thermal properties of TiO₂–epoxy NCs were compared using a universal testing machine, scanning electron microscopy (SEM), Fourier-transform infrared spectroscopy (FT-IR), and differential scanning calorimetry (DSC). The tensile strength of the NCs was improved by the dispersion strengthening effect of the TiO₂ nanoparticles, and focused sonication improved the tensile strength the most when nano-TiO₂ suspensions with a particle size of 100 nm or smaller were used. Thus, the reinforcing effect of TiO₂ nanoparticles on the epoxy resin was observed, and the nano-TiO₂ suspension produced by focused sonication showed a more distinct reinforcing effect.

Keywords: polymer nanocomposites; dispersoid; nano-TiO₂ suspensions; ultrasonic dispersion; focused ultrasonication



Citation: Choi, Y.-M.; Hwangbo, S.-A.; Lee, T.G.; Ham, Y.-B. Effect of Particle Size on the Mechanical Properties of TiO₂–Epoxy Nanocomposites. *Materials* **2021**, *14*, 2866. <https://doi.org/10.3390/ma14112866>

Academic Editors: Alfonso Maffezzoli, Alessandro Pegoretti and Michał Strankowski

Received: 31 March 2021

Accepted: 24 May 2021

Published: 27 May 2021

Publisher's Note: MDPI stays neutral with regard to jurisdictional claims in published maps and institutional affiliations.



Copyright: © 2021 by the authors. Licensee MDPI, Basel, Switzerland. This article is an open access article distributed under the terms and conditions of the Creative Commons Attribution (CC BY) license (<https://creativecommons.org/licenses/by/4.0/>).

1. Introduction

Epoxy resin (EP) is an important industrial material that has many applications in the electronics, automobiles, and aerospace fields, owing to its high strength and stiffness, resistance to chemicals, low contraction during curing, excellent corrosion resistance, and thermal characteristics [1–3]. However, its other characteristics such as brittleness, poor resistance to crack propagation, and low wear resistance limit its applications [4–6]. To this end, several studies have investigated various fillers that can be added to improve the properties of the matrix.

Composite technology and nanotechnology are being extensively researched to solve these chronic problems that cannot be solved using single-layer materials. Nanocomposite technology has gained considerable research interest in all disciplines including engineering, physics, chemistry, and medicine; furthermore, it is believed to promote technical development in various fields such as information, electronics, materials, and energy [7]. Nanocomposites (NCs) reinforced with nanosized materials (1–100 nm size distribution) can be applied to a variety of materials including polymer-based NCs. Polymer nanocomposites (PNCs) are produced by combining lightweight, flexible polymers with low production costs as a matrix with inorganic nanoparticles that exhibits excellent mechanical and electromagnetic properties [8–10]. A PNC is a polymer matrix modified with reinforcement nanoparticles at a low ratio (<5.0 wt.%). Various nanoparticles, such as

carbon nanotubes, titania (TiO₂), silica, and alumina are used as the reinforcement particles [11–14]. These PNCs exhibit excellent mechanical, physical, and chemical properties; however, these properties strongly depend on the interfacial bond strength between the polymer matrix and reinforcement particles. The cohesion of nanoparticles and the high viscosity of polymers makes it considerably difficult to uniformly disperse nanoparticles of 5 wt.% or lower. Therefore, a mechanism that can uniformly disperse nanoparticles in a highly viscous liquid is highly desirable in academic circles [15–17].

The performance of nanoparticle-reinforced PNCs as a function of dispersion and interfacial interaction has been investigated in many studies; the results have suggested that good dispersion and strong interfacial interaction can effectively transfer the stress from the polymer matrix to the nanomaterials [18,19]. Various dispersion methods such as extrusion, ball milling, three-roll milling, solvent casting, and functionalization of nanoparticles have been employed. Among these methods, the mechanical mixing method is most commonly applied to create violent mixing, thereby generating turbulence on a large scale to nanoparticles. However, this method cannot prevent nanoparticle aggregation into the polymer matrix [20–22]. Therefore, ultrasonic dispersion methods are used instead of mechanical mixing methods to achieve high homogeneity [23,24]. Ultrasonic waves are classified into low- and high-frequency waves; the latter can decompose aggregates and separate particles accumulated on the microchannel surface by generating cavitation microbubbles. In contrast, the former form an ultrasonic sound field and lead to acoustic radiation and streaming effects, which facilitates biological and chemical treatments such as cell separation and fluid mixing [25–29]. Ultrasonic cavitation is an effective method for dispersing nanoparticles. As compression and rarefaction cycles are switched sequentially, high-intensity ultrasonic waves spread to the liquid polymer matrix; simultaneously, microbubbles of vacuum are created and collapsed in the matrix. When these microbubbles collapse, the local temperature changes to 10⁵ Ks^{−1} because of the shockwave, and a pressure of several megapascals is generated. This energy can be used to disperse nanoparticles [30,31].

This study compared the dispersion of nano-TiO₂ suspensions using three types of ultrasonic systems (bath sonication, probe sonication, and the novel focused sonication method we developed and reported in a previous paper [32]) to verify the nanoparticle dispersion efficiency of a proprietary focused sonication system. In detail, focused ultrasound uses cylindrical piezoelectric ceramics to dissolve agglomeration through the energy collected in the center. Generally, the surface charge of particles that prevent agglomeration is improved, to have a zeta potential value of about 40–50 mV in the dispersion process, which ensures long-term dispersion stability that does not re-aggregate for more than 1 year. We had confirmed that even when lyophilized particles were re-dispersed in water, they were dispersed to less than 100 nm without aggregation. Thus, the NCs based on EP were produced using the nano-TiO₂ suspensions obtained by each ultrasonication method in this study; then, the physical properties of the TiO₂–epoxy NCs were compared based on the added amount.

2. Experiment

2.1. Materials

TiO₂ nanoparticles used in this study were type P25 (CAS: 13463-67-7) purchased from EVONIK Co. Ltd. (Essen, Germany); they had an average particle size of 25 nm and a density of 3.78 g/cm³. Figure 1 shows the shape of the TiO₂ nanoparticles observed using transmission electron microscopy (TEM) (JEM-ARM200F, JEOL, Tokyo, Japan).

The polymer matrix was produced by mixing an EP and hardener supplied by Kukdo Chemical Co. Ltd. (Seoul, Korea). YD-128 (CAS: 25068-38-6) of the bisphenol-A type was used as the EP, and KBH-1085 (CAS: 25134-21-8) of nadic methyl anhydride (NMA) was used as the hardener. An accelerator (CAS: 103-83-3) of benzyl dimethyl amine (BDMA) was used as the hardening accelerator and was supplied by NEW SEOUL CHEMICAL (Seoul, Korea). YD-128, KBH-1085, and the accelerator were mixed at a manufacturer-

recommended weight ratio of 100:60:2.5. Figure 2 shows the molecular structures of the EP, hardener, and hardening accelerator.

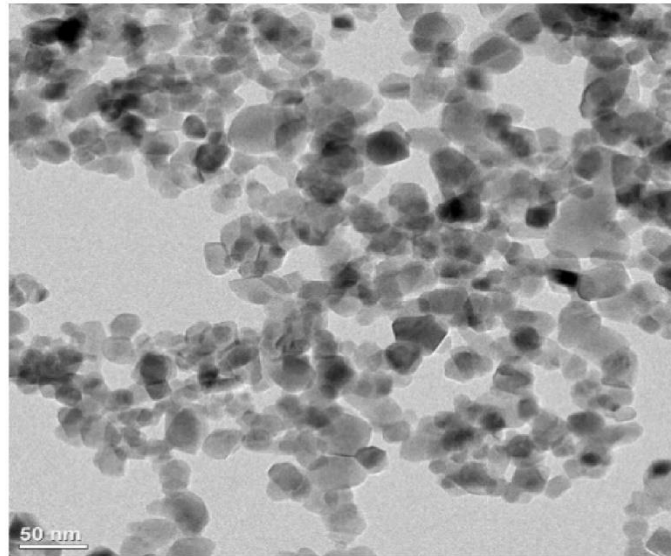
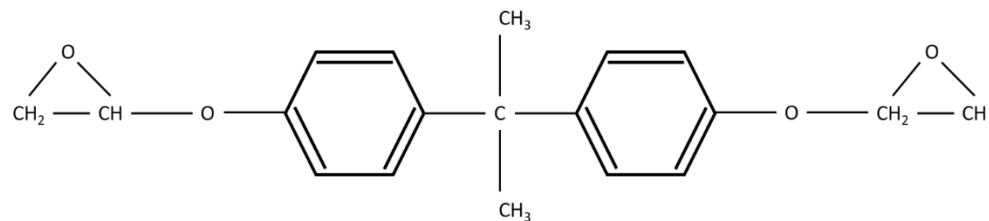
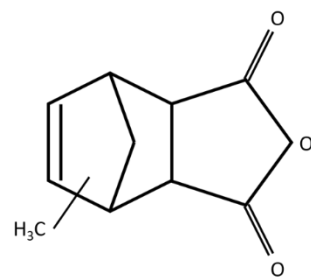


Figure 1. TEM image of the P25 purchased from EVONIK Co., Ltd.

(a) Epoxy resin (YD-128)



(b) NMA (KBH-1085)



(c) BDMA (accelerator)

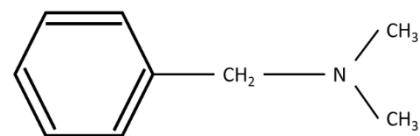


Figure 2. Chemical structures of (a) epoxy resin, (b) hardener, and (c) hardening accelerator.

2.2. Sample Preparation

In this study, the PNC was produced by dispersing TiO₂ nanoparticles (1.0 wt.%) in 100 mL of the deionized water and by adding it into a matrix. The nano-TiO₂ suspension was dispersed using bath-type, probe-type, or focused-type sonication. SD-300H (Sungdong Ultrasonic Co., Seoul, Korea) and Branson SFX 550 (Emerson Co. Ltd., Saint Louis, MO, USA) were used for bath- and probe-type sonication, respectively. The results were compared with those of a proprietary focused sonication system [32].

Delivered sonic energy (DSE) (J/mL) is an important parameter in ultrasonication; it is the actual ultrasonic energy delivered to the sample. The mean particle size of TiO₂ when DSE was applied to the same volume is compared in this study [33]. The DSE was calculated using

$$P = (dT/dt)MC_p, \quad (1)$$

$$DSE = P \times (t/V), \quad (2)$$

where P , dT/dt , M , C_p , t , and V denote the ultrasonic energy obtained by the calorimetric method [J/s], variation in temperature at time t [K/s], mass of the solution [g], heat capacity of water, time [s], and volume of the solution (mL), respectively.

The DSEs obtained using the three types of sonication methods are summarized in Table 1. To verify the particle size distribution of the TiO₂ suspension dispersed at different ultrasonic energies, the mean particle size was measured after ultrasonication using dynamic light scattering (Zetasizer Nano ZS, Malvern Panalytical Ltd., Malvern, UK).

Table 1. Specifications of the three types of sonication methods.

Specification	Bath Sonication	Probe Sonication	Focused Sonication
Frequency	40 kHz	20 kHz	400 kHz
Solution volume	100 mL	100 mL	100 mL
Irradiation time	32 h 12 min	1 h 47 min	2 h
Ultrasonic energy (P)	1.7 J/s	29.6 J/s	27.0 J/s
Delivered sonic energy (DSE)	194.7 J/mL	194.7 J/mL	194.7 J/mL
Median particle size	206.8 nm	155.3 nm	96.4 nm
Range of particle size distribution	122–5560 nm	60–531 nm	37.8–255 nm

The particle size of TiO₂ was 25 nm; however, it was agglomerated to approximately 500 nm [34]. After dispersion with the three sonication methods, the mean sizes of the nanoparticles were 96.4 nm, 155.3 nm, and 206.8 nm, as shown in Figure 3. Nano-TiO₂ suspensions with a diameter of 100 nm were produced when the particles were dispersed by focused sonication. Furthermore, the intensity of the size distribution was higher than that of the others, which indicated that the particle sizes were more uniform because of the focused sonication.

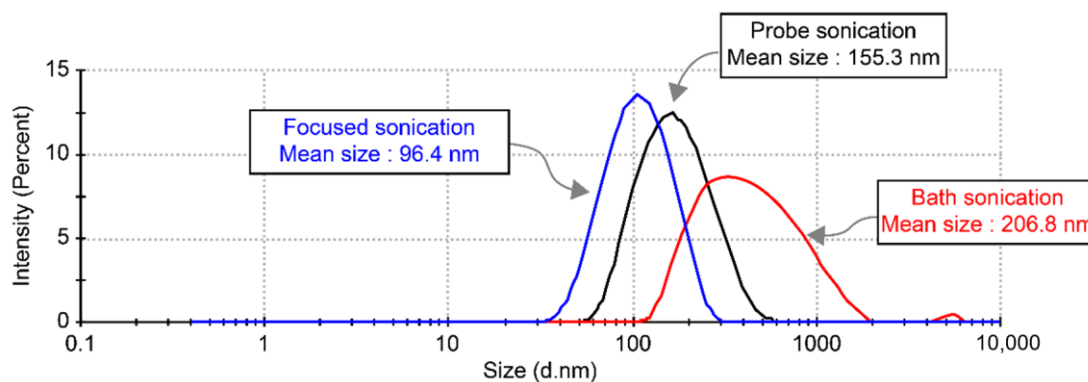


Figure 3. Size distribution of TiO₂ nanoparticles in deionized water based on sonication type.

Figure 4 shows an overview of the PNC manufacturing process. In this study, NCs with four different compositions were manufactured by adding nano-TiO₂ suspensions (0.5 wt.%, 1.0 wt.%, 3.0 wt.%, and 5.0 wt.%) to an EP. It was difficult to disperse the EP with nanoparticles because of its high viscosity; therefore, the EP and TiO₂ suspensions were dispersed using a stirring device and probe-type sonication. After mixing for 30 min at 293.15 K using a mechanical agitator OS20-Pro (Korea Process Technology Co., Ltd., Seoul, Korea), they were dispersed for 180 min at 293.15 K using an ultrasonic dispersion system VC-505 (Sonics & Materials Inc. (Newtown, CT, USA)). The residual gas was removed from the EP with a TiO₂ suspension dispersed through a degassing process for 180 min in a 333.15 K vacuum oven. Then, the hardener and hardening accelerator were added and mixed for 5 min by hand stirring to blend and evenly distribute it with minimal bubbles; an additional degassing process was applied for 30 min in a 333.15 K vacuum

oven. The TiO₂-epoxy NCs were fabricated as tensile specimens (shape and dimensions as shown in Figure 5) hardened in two steps of 398.15 K for 60 min and 423.15 K for 180 min (Figure 4).

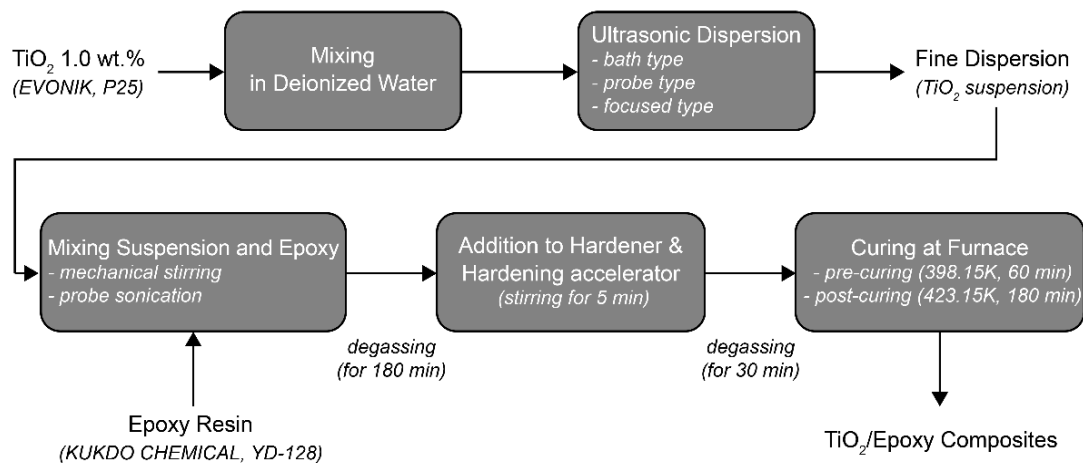


Figure 4. Flowchart of TiO₂-epoxy nanocomposite preparation.

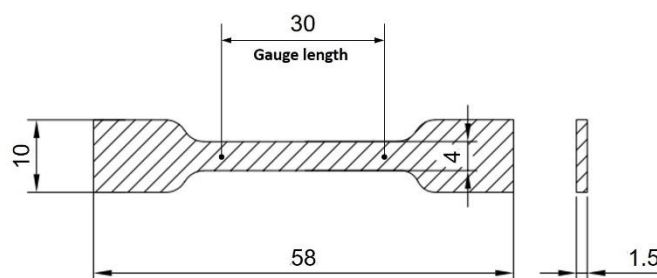


Figure 5. Dimensions for the tensile test specimen.

2.3. Characteristics of the Nanocomposites

The mechanical properties of 12 different batches of TiO₂-epoxy NCs (namely, four different compositions and three different sonication methods) were measured using tensile tests and compared with those of pure epoxy resin samples. As shown in Figure 5, eight specimens per batch were molded into dog-bone-shaped tensile test specimens, which were tested in the tension mode of a universal testing machine M350-10CT (Testometric Co. Ltd., Rochdale, UK) at a crosshead speed of 2 mm/min. Then, the five median values were determined from each batch of eight samples, and the average of these five median values was calculated. In addition, the fracture surface was analyzed using SEM (SEM; SU5000, Hitachi, Tokyo, Japan) after the tensile test.

The thermal properties of one sample per batch were examined using DSC, which can analyze thermal properties such as glass transition temperature, crystallization temperature, and melting temperature using the calorie difference based on the temperature gradient between the reference material and the sample. Quantitative data can be obtained from the positions, shapes, and areas of the peaks in a DSC curve. In this study, the thermal properties of pure epoxy and TiO₂-epoxy NCs were analyzed using the Perkin Elmer Diamond model (Perkin Elmer, Waltham, MA, USA) at a heating rate of 10 K/min from 273.15 K to 673.15 K in a nitrogen (N₂) atmosphere.

Attenuated total reflectance Fourier-transform infrared (ATR-FTIR) spectroscopy was also used on one sample per batch to verify the bonding structure of the samples. ATR-FTIR spectroscopy is useful for measuring the surfaces of polymers such as sponges and adhesives, which are difficult to process. The IR beam from the interferometer is transmitted into a diamond crystal that results in an internal reflection at the boundary with the sample, because it has a greater refractive index than the sample in contact on

both sides. Meanwhile, the IR spectrum that reflects the vibration and rotational motions of molecules are measured, and a qualitative analysis of the sample including molecular species is performed. The pure epoxy and TiO₂-epoxy NCs were analyzed using ALPHA-P (Bruker, Billerica, MA, USA); the ATR-FTIR spectra were collected by scanning the sample surface in the range of 400–4000 cm⁻¹.

3. Results and Discussion

3.1. Mechanical Properties of Nanocomposites

Dog-bone-shaped specimens were fabricated, and the tensile strengths were measured to examine the changes in the mechanical properties of the TiO₂-epoxy NCs. Figure 6 shows the average tensile strengths of the NCs after sonication of the nano-TiO₂ suspension. The average tensile strength of the composites with the nano-TiO₂ suspension added was up to 15% higher than that of the pure EP. In particular, the tensile strengths of the NCs with 1.0 wt.% nano-TiO₂ suspension processed by focused sonication was higher (92.9 MPa) compared to those processed using probe sonication (91.1 MPa) or bath sonication (89.7 MPa). Usually, bath sonication can handle large amounts at once, although it has been known to be less efficient at dispersion, and probe sonication has a strong irradiation energy, but it also has blind spots such as on the upper side of the probe. On the other hand, compared with the former sonication methods, it was determined that focused sonication had a positive effect on the TiO₂ dispersion in the EP matrix. Due to the driving characteristics of focused sonication, it could continuously apply ultrasonic energy to the circulating object [32].

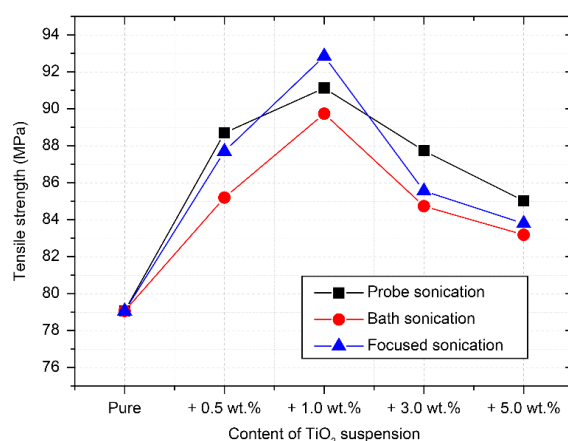


Figure 6. Tensile strength of the TiO₂-epoxy nanocomposites in accordance with the sonication method.

The tensile strength of the composites tended to decrease gradually when the added amount of nano-TiO₂ suspension that passed through the ultrasonic dispersion system was 3.0 wt.% or higher. The decreased tensile strength of the NCs reinforced with nano-TiO₂ suspension above a certain amount seems to be attributed to the following two problems: (1) The deionized water among the component materials of the nano-TiO₂ suspension fabricated in this study had an adverse effect on the polymerization process of the EPs with hydroxyl and carboxyl groups. Therefore, the residual water in the TiO₂-epoxy NCs needed to be checked via thermal analysis and the improvements should be identified [35,36]; (2) The interference of the epoxy polymerization and the reduced effect of particle reinforcement was attributed to the agglomeration of TiO₂ nanoparticles. Adding a large quantity of nanoparticles into a highly viscous EP causes agglomeration because of the attraction between particles. Accordingly, the agglomerated nanoparticles serve as impurities in the resin; therefore, they decrease the mechanical properties [37–39]. In this study, when PNCs were produced by adding a nano-TiO₂ suspension produced by the same sonication method in the range of 0.5–5.0 wt.%, the addition of 1.0 wt.% was found to be the optimal amount.

3.2. Microstructural and Morphological Analysis

Microstructures at $200\times$ magnification were observed using SEM to examine the failure behavior of the TiO_2 -epoxy NCs. Figure 7 shows the fracture surface images after the tensile testing of pure EP and epoxy NCs reinforced with TiO_2 using different sonication methods. Pure EP was very clear: from Figure 7a, the fracture surface of neat epoxy showed a very smooth pattern where cracks propagated arbitrarily without restraint, indicating the brittle fracture of neat epoxy without resistance to crack initiation and transmission. Compared to the fracture surface of the pure EP, the fracture surface of NCs with TiO_2 nanoparticles added in Figure 7b–d showed a rough cliff-like pattern (blue arrow: flat cross-section, and red arrow: rough cross-section). In general, more fracture energy is dissipated for greater roughness. These observations reveal the generation of a rough surface by the deflection of propagating crack fronts on the loading of TiO_2 in the EP matrix. In other words, the cracks progressed relatively rapidly without high resistance at the fracture surface of the pure epoxy specimen; furthermore, the crack resistance of the TiO_2 -epoxy NCs improved with the addition of nanoparticles, which acted as a factor that increased the tensile strength [40,41].

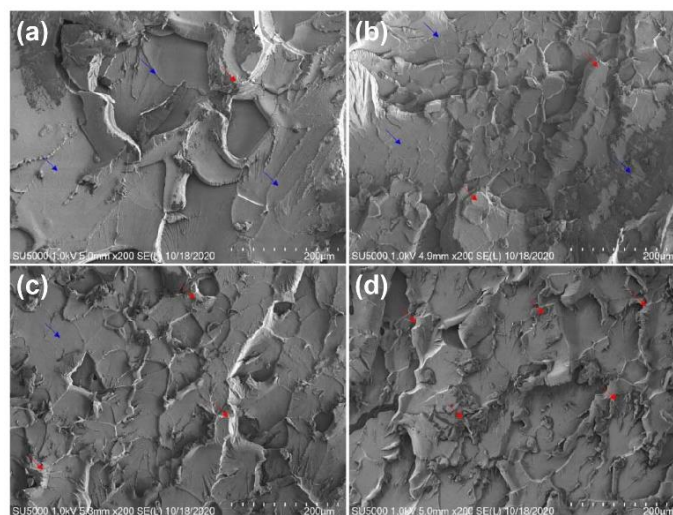


Figure 7. SEM images of (a) the pure epoxy resin and the 1.0 wt.% TiO_2 -epoxy nanocomposites with (b) bath sonication, (c) probe sonication, and (d) focused sonication.

Figure 8 shows the SEM images with $500\times$ magnification for the fracture surfaces of the nanocomposite reinforced with nano- TiO_2 suspension dispersed by focused sonication. The characteristic brittleness and low fracture toughness of the pure epoxy are a product of their high cross-link densities, which resulted in the poor absorption of energy during the fracture. These factors frequently lead to mirror-like fracture surfaces, as shown in Figure 8a. Changes in the fracture surface caused by the added nanoparticles were examined. Compared to that for the pure epoxy, the fracture surface of NCs contained greater roughness, as shown in Figure 8b–e. The coarse multiplane features on the TiO_2 -epoxy NCs fracture surface suggest that the TiO_2 nanoparticles induced the deflection of propagating crack fronts. Furthermore, NCs with 3.0 wt.% and 5.0 wt.% TiO_2 showed a decreased roughness compared to the NCs with 1.0 wt.% nano- TiO_2 suspension. The PNCs are effective only if the nanoparticles are well dispersed in the surrounding polymer matrix. In addition, the agglomeration of nanoparticles should not be overlooked, because nanoparticles provide a very specific surface area in the polymer matrix [10]. In other words, over-addition of nanoparticles causes the agglomeration of particles, which reduces the particle reinforcement effect. Consequently, the tensile strength could be decreased, as shown in Figure 6 above.

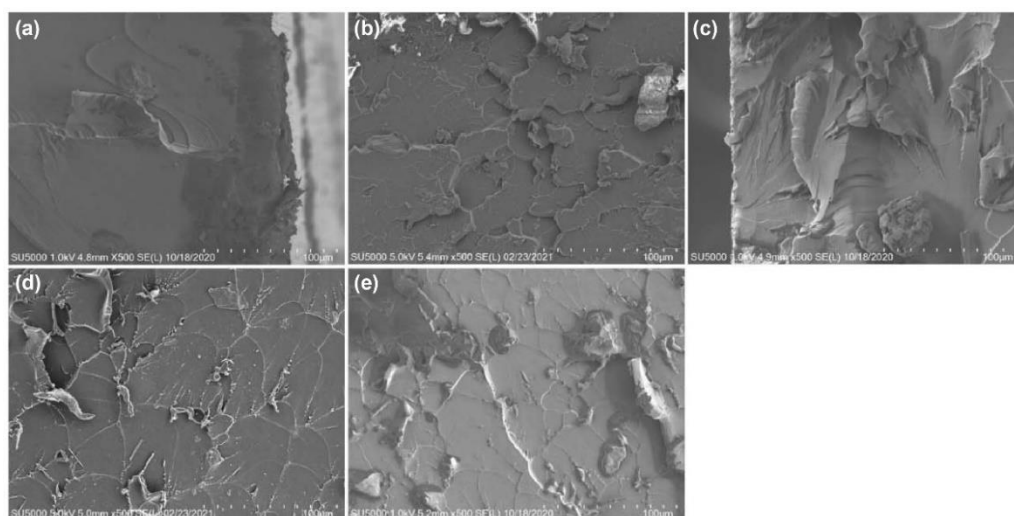


Figure 8. SEM images of (a) pure epoxy resin, (b) 0.5 wt.%, (c) 1.0 wt.%, (d) 3.0 wt.%, and (e) 5.0 wt.% TiO_2 -epoxy nanocomposites with focused sonication.

3.3. FT-IR Spectroscopy

In this study, PNCs were produced using nano- TiO_2 suspensions processed by different sonication methods but with the same content, and their physical properties were compared. As listed in Table 1, the particle size varied according to the sonication method used. The focused sonication showed an average particle size of 96.4 nm, which is smaller than those of other sonication methods. In general, crosslinking density and hydrogen bonding density are significantly affected by the content and size of the nanoparticles and the packing density in the polymer matrix. Therefore, singularities based on the bonding type and added amount of TiO_2 in the polymer nanocomposite network were examined by FT-IR analysis.

Figure 9 shows the FT-IR spectra of pure epoxy and TiO_2 -epoxy NCs in the range of $400\text{--}4000\text{ cm}^{-1}$. The O-H bond could appear at $3500\text{--}3000\text{ cm}^{-1}$, and H-O-H bonds are normally detected at $1700\text{--}1200\text{ cm}^{-1}$. These bonds could occur in the presence of water, and the results of FT-IR analysis are shown in this study. Therefore, it is assumed that there was no residual water. The peaks at $2850\text{--}2950\text{ cm}^{-1}$ indicated the C-H group, whereas those at $1730\text{--}1740\text{ cm}^{-1}$ and 1510 cm^{-1} indicated the C=O and aromatic groups, respectively. The TiO_2 -epoxy NCs processed by focused sonication showed peak intensities similar to those of pure epoxy. Overall, the FT-IR patterns of all samples including the pure EP were almost the same, which suggests that there was no chemical bonding between TiO_2 and the EP.

3.4. Thermal Property of Nanocomposites

Nanoparticles play a key role in improving the thermodynamic properties of EPs. Among them, TiO_2 is widely used in industries because of its diverse functions and synthesis methods. The state of materials can be analyzed using DSC based on temperature changes with high speed and precision, and it is used in research investigating the physical properties of polymers. In particular, DSC is widely used for examining polymeric materials to determine their thermal transitions. Important thermal transitions include the glass transition temperature (T_g), crystallization temperature (T_c), and melting temperature (T_m). The epoxy resin of bisphenol-A-type, an amorphous polymer, was used in this study; thus, we expected to obtain acceptable T_g and T_m values. The T_g is a very important thermal property in polymeric systems. The unit of polymers is a certain segment in the molecular chain, and the thermal motion by the rotation of this segment is called micro-Brownian motion. The temperature at which micro-Brownian motion starts is called the glass transition temperature, and it is also referred to as the second transition temperature, which is a unique property of polymers.

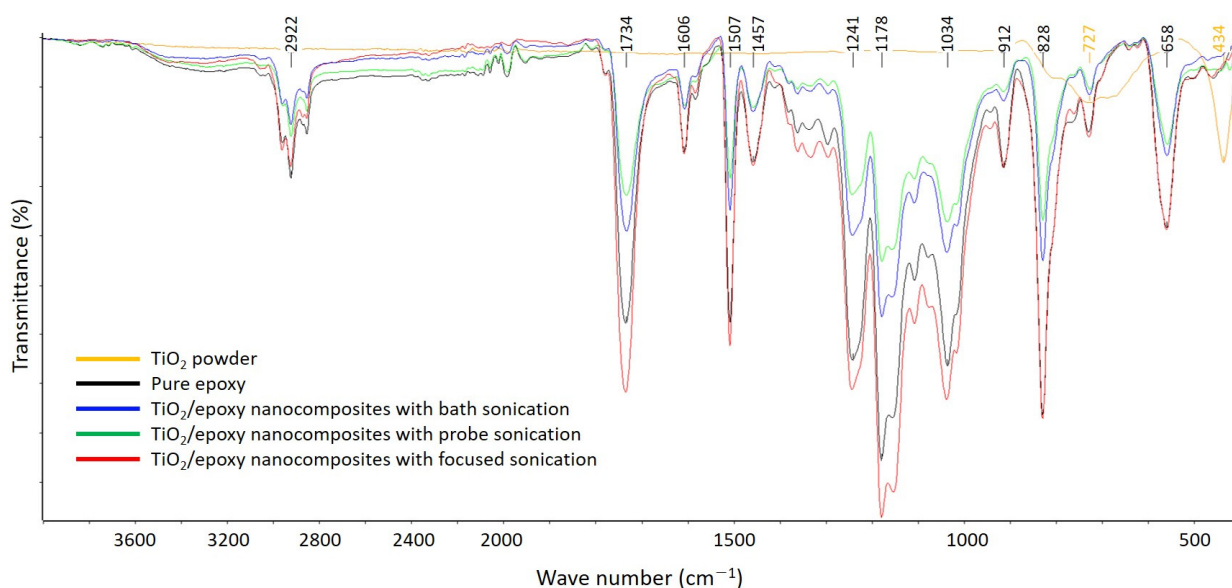


Figure 9. FT-IR spectra of the TiO_2 powder, pure epoxy resin, and the 1.0 wt.% TiO_2 -epoxy nanocomposites.

Figure 10 shows the DSC curves of the pure epoxy and TiO_2 -epoxy NCs. A glass transition point was observed at 350–450 K, wherein the endothermic reaction of pure EP appeared distinctly. The glass transition temperature of the pure EP is 355 K. Furthermore, the glass transition temperatures of the NCs processed by focused sonication, probe sonication, and bath sonication were 400.0 K, 375.7 K, and 360.0 K, respectively. This confirmed that the thermal properties of the TiO_2 -epoxy NCs were improved compared to those of the pure EP [42,43]. The NCs in which the nano- TiO_2 suspensions were dispersed by focused sonication showed the best thermal properties, and therefore, thermal stability could be expected.

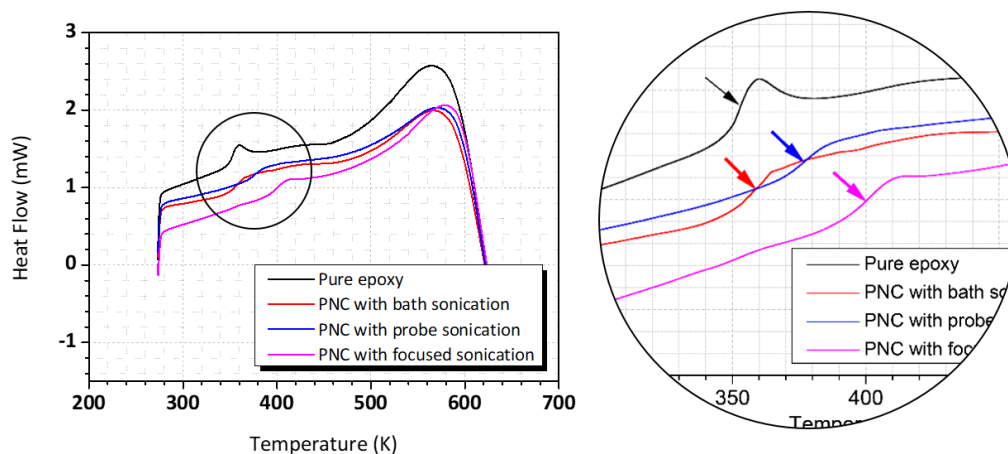


Figure 10. DSC curve of the 1.0 wt.% TiO_2 -epoxy nanocomposites in accordance with the sonication method conducted within the range of 200–700 K.

On the other hand, there were no other reactions than phase transitions of the nanocomposites. We fabricated the nanocomposites using an aqueous solution-based TiO_2 suspension in this study, and we have confirmed that the residual moisture could have an adverse effect on the nanocomposites. However, compared to pure epoxy resin, the specificity peak of nanocomposites was not shown in the DSC analysis.

4. Conclusions

In this study, the effect of TiO₂-epoxy size on the mechanical properties of particle NCs was investigated. In addition, nano-TiO₂ suspensions were dispersed separately using the existing bath sonication and probe sonication methods to examine the dispersion efficiency of a proprietary focused sonication dispersion system. A nano-TiO₂ suspension with a mean particle size of 96.4 nm was obtained using the focused sonication dispersion system. TiO₂ particle-reinforced epoxy NCs were fabricated, and their mechanical properties were compared. The following conclusions could be drawn based on the results.

1. The tensile strength of the TiO₂-epoxy NCs was improved compared to that of the pure EP. The highest tensile strength was observed when 1.0 wt.% of TiO₂ suspension (mean particle size 100 nm or lower) dispersed by focused sonication was added. However, the tensile strength of more than 3.0 wt.% TiO₂-reinforced epoxy NCs decreased regardless of particle size;
2. The SEM analysis of the fracture surface indicated that the crack resistance of the TiO₂-epoxy NCs was greater than that of the pure EP; this influences the tensile strength;
3. The FT-IR spectra of the pure EP and TiO₂-epoxy NCs were almost the same, which suggests that chemical bonding with TiO₂ did not occur. The TiO₂-epoxy NCs showed improved thermal properties compared to pure EP;
4. The glass transition temperature of the TiO₂-reinforced epoxy NCs with a particle size of 100 nm or less (dispersed by focused sonication) was the highest at 400 K; this implies that the performance improvement of the nanocomposite was affected by the size of the nanoparticles;
5. Both the tensile strength and thermal properties improved when a suspension with a particle size of 100 nm or less was used; this was confirmed to be greatly influenced by the nanoparticle dispersion method.

Continuous research is needed to further optimize and standardize the focused ultrasound method used in this study so that it can be applied to various NCs.

Author Contributions: Conceptualization, Y.-M.C. and S.-A.H.; Methodology, Y.-M.C.; Software, Y.-M.C. and S.-A.H.; Validation, Y.-M.C. and S.-A.H.; Formal analysis, Y.-M.C. and S.-A.H.; Investigation, Y.-M.C. and S.-A.H.; Resources, S.-A.H.; Data curation, Y.-M.C. and S.-A.H.; Writing—original draft preparation, Y.-M.C., S.-A.H. and Y.-B.H.; Writing—review and editing, Y.-M.C., S.-A.H., T.G.L. and Y.-B.H.; Visualization, Y.-M.C. and S.-A.H.; Supervision, S.-A.H., T.G.L. and Y.-B.H.; Project administration, S.-A.H., T.G.L. and Y.-B.H.; Funding acquisition, S.-A.H., T.G.L. and Y.-B.H. All authors have read and agreed to the published version of the manuscript.

Funding: This work was supported by the Nano-Material Technology Development Program of the National Research Foundation (NRF) funded by the Ministry of Science and ICT (grant number 2016M3A7B6908929), and the Development of Measurement Standards and Technology for Biomaterials and Medical Convergence funded by the Korea Research Institute of Standards and Science (KRISS-2021-GP2021-0004).

Data Availability Statement: Data available in a publicly accessible repository.

Conflicts of Interest: The authors declare no conflict of interest.

References

1. Ashrafi, M.; Hamadani, M.; Ghasemi, A.R.; Kashi, F.J. Improvement mechanical and antibacterial properties of epoxy by polyethylene glycol and Ag/CuO nanoparticles. *Polym. Compos.* **2019**, *40*, 3393–3401. [[CrossRef](#)]
2. Heng, Z.; Chen, Y.; Zou, H.; Liang, M. Simultaneously enhanced tensile strength and fracture toughness of epoxy resins by a poly(ethylene oxide)-block-carboxyl terminated butadiene-acrylonitrile rubber dilock copolymer. *RSC Adv.* **2015**, *5*, 42362–42368. [[CrossRef](#)]
3. Flick, E.W. *Epoxy Resins, Curing Agents, Compounds, and Modifiers: An Industrial Guide*; William Andrew: Norwich, NY, USA, 2012.
4. Shen, X.J.; Pei, X.Q.; Liu, Y.; Fu, S.Y. Tribological performance of carbon nanotube-graphene oxide hybrid/epoxy composites. *Compos. Part B Eng.* **2014**, *57*, 120–125. [[CrossRef](#)]
5. Jiang, T.; Kuila, T.; Kim, N.H.; Ku, B.C.; Lee, J.H. Enhanced mechanical properties of silanized silica nanoparticle attached graphene oxide/epoxy composites. *Compos. Sci. Technol.* **2013**, *79*, 115–125. [[CrossRef](#)]

6. Deng, S.H.; Zhou, X.D.; Zhu, M.Q.; Fan, C.J.; Lin, Q.F. Interfacial toughening and consequent improvement in fracture toughness of carbon fiber reinforced epoxy resin composites: Induced by diblock copolymers. *Exp. Polym. Lett.* **2013**, *7*, 925–935. [[CrossRef](#)]
7. Rajangam, K.; Amuthameena, S.; Thangavel, S.; Sanjanadevi, V.S.; Balraj, B. Synthesis and characterisation of Ag incorporated TiO₂ nanomaterials for supercapacitor applications. *J. Mol. Struct.* **2020**, *1219*, 128661. [[CrossRef](#)]
8. Green, K.J.; Dean, D.R.; Vaidya, U.K.; Nyairo, E. Multiscale fiber reinforced composites based on a carbon nanofiber/epoxy nanophased polymer matrix: Synthesis, mechanical, and thermomechanical behavior. *Compos. Part A Appl. Sci. Manuf.* **2009**, *40*, 1470–1475. [[CrossRef](#)]
9. Pinto, D.; Bernardo, L.; Amaro, A.; Lopes, S. Mechanical properties of epoxy nanocomposites using titanium dioxide as reinforcement—a review. *Const Build. Mater.* **2015**, *95*, 506–524. [[CrossRef](#)]
10. Chatterjee, A.; Islam, M.S. Fabrication and characterization of TiO₂–epoxy nanocomposite. *Mater. Sci. Eng. A* **2008**, *487*, 574–585. [[CrossRef](#)]
11. Raja, A.; Rajasekaran, P.; Selvakumar, K.; Raman, R.G.; Swaminathan, M. Visible active TiO₂–CdS–rGO ternary nanocomposite for enhanced photodecomposition of methylene blue. *Mater. Today Proc.* **2020**, *29*, 1125–1128. [[CrossRef](#)]
12. Bayan, E.M.; Lupeiko, T.G.; Pustovaya, L.E.; Volkova, M.G.; Butova, V.V.; Guda, A.A. Zn–F co-doped TiO₂ nanomaterials: Synthesis, structure and photocatalytic activity. *J. Alloy Compd.* **2020**, *822*, 153662. [[CrossRef](#)]
13. Takari, A.; Ghasemi, A.R.; Hamadian, M.; Sarafrazi, M.; Najafidoust, A. Molecular dynamics simulation and thermo-mechanical characterization for optimization of three-phase epoxy/TiO₂/SiO₂ nano-composites. *Polym. Test.* **2021**, *93*, 106890. [[CrossRef](#)]
14. Kumar, K.; Ghosh, P.K.; Kumar, A. Improving mechanical and thermal properties of TiO₂-epoxy nanocomposite. *Compos. Part B Eng.* **2016**, *97*, 353–360. [[CrossRef](#)]
15. Barczewski, M.; Sałasińska, K.; Szulc, J. Application of sunflower husk, hazelnut shell and walnut shell as waste agricultural fillers for epoxy-based composites: A study into mechanical behavior related to structural and rheological properties. *Polym. Test.* **2019**, *75*, 1–11. [[CrossRef](#)]
16. Alian, A.R.; Kundalwal, S.I.; Meguid, S.A. Multiscale modeling of carbon nanotube epoxy composites. *Polymer* **2015**, *70*, 149–160. [[CrossRef](#)]
17. Abdalla, M.; Dean, D.; Robinson, P.; Nyairo, E. Cure behavior of epoxy/MWCNT nanocomposites: The effect of nanotube surface modification. *Polymer* **2008**, *49*, 3310–3317. [[CrossRef](#)]
18. Kumar, A.; Kumar, K.; Ghosh, P.K.; Yadav, K.L. MWCNT/TiO₂ hybrid nano filler toward high-performance epoxy composite. *Ultrason. Sonochem.* **2018**, *41*, 37–46. [[CrossRef](#)]
19. Kumar, A.; Ghosh, P.K.; Yadav, K.L.; Kumar, K. Thermo-mechanical and anti-corrosive properties of MWCNT/epoxy nanocomposite fabricated by innovative dispersion technique. *Compos. Part B Eng.* **2017**, *113*, 291–299. [[CrossRef](#)]
20. Mallakpour, S.; Abdolmaleki, A.; Azimi, F. Ultrasonic-assisted biosurface modification of multi-walled carbon nanotubes with Thiamine and its influence on the properties of PVC/Tm-MWCNTs nanocomposite films. *Ultrason. Sonochem.* **2017**, *39*, 589–596. [[CrossRef](#)]
21. Kudo, T.; Sekiguchi, K.; Sankoda, K.; Namiki, N.; Nii, S. Effect of ultrasonic frequency on size distributions of nanosized mist generated by ultrasonic atomization. *Ultrason. Sonochem.* **2017**, *37*, 16–22. [[CrossRef](#)]
22. Maktedar, S.S.; Mehetre, S.S.; Avashthi, G.; Singh, M. In situ sonochemical reduction and direct functionalization of graphene oxide: A robust approach with thermal and biomedical applications. *Ultrason. Sonochem.* **2017**, *34*, 67–77. [[CrossRef](#)] [[PubMed](#)]
23. Mallakpour, S. Ultrasonic-assisted fabrication of starch/MWCNT-glucose nanocomposites for drug delivery. *Ultrason. Sonochem.* **2018**, *40*, 402–409. [[CrossRef](#)]
24. Mallakpour, S.; Rashidimoghadam, S. Application of ultrasonic irradiation as a benign method for production of glycerol plasticized-starch/ascorbic acid functionalized MWCNTs nanocomposites: Investigation of methylene blue adsorption and electrical properties. *Ultrason. Sonochem.* **2018**, *40*, 419–432. [[CrossRef](#)]
25. Dong, Z.; Delacour, C.; Mc Carogher, K.; Udepurkar, A.P.; Kuhn, S. Continuous ultrasonic reactors: Design, mechanism and application. *Materials* **2020**, *13*, 344. [[CrossRef](#)] [[PubMed](#)]
26. Trujillo, F.J.; Juliano, P.; Barbosa-Cánovas, G.; Knoerzer, K. Separation of suspensions and emulsions via ultrasonic standing waves—A review. *Ultrason. Sonochem.* **2014**, *21*, 2151–2164. [[CrossRef](#)]
27. Shields, C.W., IV; Reyes, C.D.; López, G.P. Microfluidic cell sorting: A review of the advances in the separation of cells from debulking to rare cell isolation. *Lab Chip* **2015**, *15*, 1230–1249. [[CrossRef](#)] [[PubMed](#)]
28. Evander, M.; Nilsson, J. Acoustofluidics 20: Applications in acoustic trapping. *Lab. Chip* **2012**, *12*, 4667–4676. [[CrossRef](#)]
29. Gelin, P.; Van Lindt, J.; Bratek-Skicki, A.; Stroobants, S.; Krzek, M.; Ziemecka, I.; Tompa, P.; De Malsche, W.; Maes, D. Focusing of microcrystals and liquid condensates in acoustofluidics. *Crystals* **2019**, *9*, 120. [[CrossRef](#)]
30. Muthoosamy, K.; Manickam, S. State of the art and recent advances in the ultrasound-assisted synthesis, exfoliation and functionalization of graphene derivatives. *Ultrason. Sonochem.* **2017**, *39*, 478–493. [[CrossRef](#)] [[PubMed](#)]
31. Ghosh, P.K.; Patel, A.; Kumar, K. Adhesive joining of copper using nano-filler composite adhesive. *Polymer* **2016**, *87*, 159–169. [[CrossRef](#)]
32. Hwangbo, S.; Kwak, M.; Kim, J.; Lee, T.G. Novel surfactant-free water dispersion technique of TiO₂ NPs using focused ultrasound system. *Nanomaterials* **2021**, *11*, 427. [[CrossRef](#)]
33. DeLoid, G.M.; Cohen, J.M.; Pyrgiotakis, G.; Demokritou, P. Preparation, characterization, and in vitro dosimetry of dispersed, engineered nanomaterials. *Nat. Protoc.* **2017**, *12*, 355–371. [[CrossRef](#)]

34. Sato, K.; Li, J.G.; Kamiya, H.; Ishigaki, T. Ultrasonic dispersion of TiO₂ nanoparticles in aqueous suspension. *J. Am. Ceram. Soc.* **2008**, *91*, 2481–2487. [[CrossRef](#)]
35. Ahmad, Z.; Ansell, M.P.; Smedley, D. Moisture absorption characteristics of epoxy based adhesive reinforced with CTBN and ceramic particles for bonded-in timber connection: Fickian or non-Fickian behaviour. *IOP Conf Ser. Mater. Sci. Eng.* **2011**, *17*, 012011. [[CrossRef](#)]
36. Antoon, M.K.; Koenig, J.L. Irreversible effects of moisture on the epoxy matrix in glass-reinforced composites. *J. Polym. Sci. Polym. Phys.* **1981**, *19*, 197–212. [[CrossRef](#)]
37. Hu, H.; Onyebueke, L.; Abatan, A. Characterizing and modeling mechanical properties of nanocomposites-review and evaluation. *J. Miner. Mater. Charact. Eng.* **2010**, *9*, 275. [[CrossRef](#)]
38. Fisher, F.T.; Brinson, L.C. Nanomechanics of nanoreinforced polymers. In *Handbook of Theoretical and Computational Nanoscience; Volume 9: Nanocomposites, Nano-Assemblies, and Nanosurfaces*; American Scientific Publishers: Karlsruhe, Germany, 2006; pp. 253–360.
39. Moniruzzaman, M.; Winey, K.I. Polymer nanocomposites containing carbon nanotubes. *Macromolecules* **2006**, *39*, 5194–5205. [[CrossRef](#)]
40. Bortz, D.R.; Heras, E.G.; Martin-Gullon, I. Impressive fatigue life and fracture toughness improvements in graphene oxide/epoxy composites. *Macromolecules* **2012**, *45*, 238–245. [[CrossRef](#)]
41. Rafiee, M.A.; Rafiee, J.; Wang, Z.; Song, H.; Yu, Z.Z.; Koratkar, N. Enhanced mechanical properties of nanocomposites at low graphene content. *ACS Nano* **2009**, *3*, 3884–3890. [[CrossRef](#)]
42. Kumar, R.V.; Koltypin, Y.; Palchik, O.; Gedanken, A. Preparation and characterization of nickel–polystyrene nanocomposite by ultrasound irradiation. *J. Appl. Polym. Sci.* **2002**, *86*, 160–165. [[CrossRef](#)]
43. Wu, C.L.; Zhang, M.Q.; Rong, M.Z.; Friedrich, K. Silica nanoparticles filled polypropylene: Effects of particle surface treatment, matrix ductility and particle species on mechanical performance of the composites. *Compos. Sci. Technol.* **2005**, *65*, 635–645. [[CrossRef](#)]